Propagation dynamics of femtosecond pulse through subwavelength metallic hole arrays

H. M. Su, Z. H. Hang, Z. Marcet, H. B. Chan, C. T. Chan, and K. S. Wong

Phys. Rev. B **83**, 245449 — Published 29 June 2011

DOI: 10.1103/PhysRevB.83.245449

Propagation dynamics of femtosecond pulse through subwavelength metallic hole arrays

H. M. Su,[1] Z. H. Hang,[1] Z. Marcet,[1, 2] H. B. Chan,[1, 2] C. T. Chan,[1] and K. S. Wong[1]*

[1] Department of Physics, the Hong Kong University of Science and Technology, Kowloon, Hong Kong, People's Republic of China

[2] Department of Physics, University of Florida, United States

We have studied the frequency-dependent transmission time delay of femtosecond (fs) laser pulses through subwavelength hole arrays in aluminum films using the up-conversion technique. The pulse delays measured at different wavelengths mainly follow the far-field transmission profile of the surface plasmon polariton (SPP) resonances. Temporal delays of 60fs and 100fs were found at the major SPP resonance in the single-layer and double-layer samples. A coupled-SPP transmission model is used to explain the temporal dynamics of the transmission process. Our experiment shows that the weak coupling between the SPP waves on different metal/dielectric interfaces leads to the large temporal delay of the transmitted pulses.

PACS number(s): 42.25.Bs; 42.79.Dj; 78.67.-n; 52.38.-r

[*] Corresponding author: phkswong@ust.hk

I. INTRODUCTION

The observation of extraordinary optical transmission[1] (EOT) through subwavelength holes in metal films has sparked intense experimental and theoretical investigations in recent years. Not only can the transmission be orders of magnitude larger than expected from classic diffraction theory, but also the peak positions in the transmission spectrum can be tuned by adjusting the period of the hole array, the hole size and the thickness of the film. Moreover, the concentration of light in the subwavelength apertures leads to an electric field enhancement which can be used to manipulate the light-matter interactions and nonlinear processes. These effects hold promise in a wide range of applications in the area of science and technology such as near-field microscopy, nanosize laser sources, femtosecond electron sources, nanolithography, optical modulators, biosensor, and display devices.[2-8]

The large transmission enhancement has been attributed to a resonant interaction of the incident light with the SPP modes at the metal surface.[9, 10] For subwavelength holes or slits in a metal film, two distinct paths contribute to the total transmission. The first path is non-resonant scattering of the incident field towards the scattered states through the holes or slits. This part of transmission is spectrally flat or slowly varying. The second path corresponds to a resonant channel via a discrete SPP excitation in the structure. In the spectral domain, the interference between the resonant and the non-resonant channel gives rise to an asymmetric line shape, the Fano profiles, in the far field transmission spectrum.[11] The linewidth of the SPP mode (Γ) can be estimated from the Fano-line-shaped peaks and related to the SPP lifetime as $T_1 = (2\Gamma)^{-1}$.[12-17] Correspondingly in the time domain, the SPP-photon coupling leads to distortion and propagation delay of the light pulses at the SPP resonance

through the structures. The transmission dynamics of EOT have been studied theoretically[13, 18-21] and experimentally.[12, 16, 22] A 7-fs pulse transit time was measured through the subwavelength hole array in a 300nm thick silver film at the SPP resonance, indicating a group velocity of $c/7$.[12] A severe pulse distortion was found in the temporal profile of a femtosecond laser pulse propagating through a metallic plasmonic crystal at the long-life SPP resonances.[16] Both theoretical modeling[13, 20, 21] and femtosecond time-resolved measurements[14] have observed a two-component structure in the temporal evolution of the transmitted pulse through the subwavelength hole or slit array: a fast transmission of a nearly unperturbed pulse followed by a long tail. Such structures are the temporal fingerprint of a Fano-type process. Moreover due to the coupling between multiple interfaces, the transmitted pulse exhibits oscillations at the femtosecond time scale. Both the period and the damping of these oscillations were determined by the coupling strength between the interfaces.[19] It has also been shown that the radiative lifetime of SPP mode is limited by the SPP scattering at the periodic array.[14, 21] Hence the temporal behaviors of the light pulses through diffraction gratings can provide insight into the dephasing dynamics of surface plasmon modes and the role of the grating structure in the transmission processes, which are crucial for the proposed application of plasmon-based photonics.

In this paper, we present experimental investigations on femtosecond laser pulses transmitted through single- or double-layer aluminum films perforated with subwavelength hole arrays. Temporal delays of light pulses from 1.5μm to 1.7μm, at the optical fiber communication window, have been measured to study the SPP-photon interaction, as well as the influence of the structure on the SPP damping dynamics. The coupling effect between SPP waves at multiple interfaces is discussed with a coupled SPP transmission model. Among different studies of light transmission

through perforated metal films, the geometric dependence of SPP modes and the interaction between SPP waves are usually investigated in the frequency domain. Only a few theoretical papers deal with the light transmission dynamics with SPP coupling via photon tunneling through the nanoapertures.[19, 21] Our experiment shows that the weak coupling between the SPP waves on different interfaces is responsible for the long delay time of the transmitted pulses.

II. EXPERIMENTAL PROCEDURE

The single-layered (sample A) and double-layered (sample B and C) aluminum films of 0.39μm in thickness are embedded in silicon oxide ($n \approx 1.47$) and placed on top of the quartz substrate.[23] Each aluminum layer is perforated with a 2D square array of holes by lithographically patterning a photoresist layer followed by reactive ion etching into the aluminum. The hole diameter is about 0.5μm on the top surface and 0.42μm on the bottom surface. The period of the square array is 1.0μm. In the double layer samples, the spacing between the two aluminum layers is 0.3μm, and the square holes array of the 2 layers are either aligned (sample B) or with a lateral shift of 0.5μm in the x direction (sample C, Fig. 1a). The detailed fabrication procedure of these structures can be found in our previous work.[23]

The temporal profiles of femtosecond laser pulses propagating through the samples were measured using the up-conversion technique. A Ti: sapphire amplifier was used to deliver optical pulses at a center wavelength of 800nm with pulse duration of 150fs. The pulses were then split into two parts. One part went through an optical delay line, and the second harmonics (SH) of the other part was used to pump a home-made optical parametric generation/amplification (OPG/OPA) system.[24] The idle branch (infrared, IR) of the OPG/OPA system, with the center wavelength

tunable from 1.49μm to 1.7μm, was slightly focused onto the sample from the quartz substrate side in the normal direction. The transmitted light through the sample was then collected and forwarded to a Beta-Barium Borate (β-BaB_2O_4, BBO) crystal together with the laser pulses from the delay line. When the laser beam from the delay line and the transmitted pulses through the samples were present simultaneously in the BBO crystal, frequency mixing occurred, resulting in the generation of an up-converted signal.[25] The up-converted signals were measured at different delay time using a photodiode and a lock-in amplifier (Fig.1b).

Figure 2 shows the detected up-converted signal with pulses at 1.548μm. The spectrum of the incident pulses (inset of Fig. 2) shows a full width at half maximum (FWHM) of about 30nm. The black curve marked '*Substrate*' is the up-converted signal measured with pulses propagating through a blank area on the SiO_2/quartz substrate without aluminum structures. In the rest of this paper, the measured up-converted signals of the '*Substrate*' are taken as references to deduce the relative time delays of pulses through the single and double layer samples. The curve '*SL*' refers to the single layer hole array (sample A). '*D0*' is for the double layer sample with aligned hole arrays (sample B). Both '*DX*' and '*DY*' are referred to the double layer hole array with 0.5μm lateral shift between layers in the x direction (sample C). *DX* was measured with the incident light polarized in the x direction (parallel to the lateral shift) and *DY* with the incident light polarized in the y direction.

III. RESULTS AND DISCUSSION

A. SPP Resonance

The far-field transmission spectra of sample A shows one major SPP resonant peak at 1.53μm.[23] For the double-layered samples, two SPP modes are found, with

SPP mode 1 at around 1.53μm and *SPP mode 2*, the guided mode, above 1.58μm.[23] The resonant frequency of the latter depends strongly on the lateral shift between the hole arrays on the two layers. Figure 3 shows our Finite-Different Time-Domain (FDTD) simulations (Concerto 6.5, by Vector Field Inc.) of the tangent magnetic field distribution of the two SPP modes in the double-layered samples. The dielectric function of aluminum was described by the Drude model with parameters extracted from the infrared optical response of aluminum. The magnetic field of *SPP mode 1* distributed largely on the two outer Al/SiO_2 interfaces (Fig. 3a and 3c), which resembles the field distribution of the symmetric SPP mode in the single layer structure. The field of *SPP mode 2* is concentrated in the gap between the two aluminum layers (Fig. 3b and 3d). Similar to the magnetic field distribution, the corresponding E_z distribution of *SPP mode 2* is present largely within the dielectric gap between the two layers and the surface charges are confined on the two inner surfaces.[23]

B. Pulse Transmission Delays

Figure 4 shows the measured pulse delay at different wavelengths together with the far-field transmission spectra and the corresponding Fano line shape fittings. Because of the spectral width of the incident pulses and the laser power fluctuations, the overall systematic error were up to ±5fs in our experiments at some wavelengths. Negative time delays are occasionally recorded due to the non-uniform thickness of the substrate between different samples or within one sample. As shown in Fig.4, the magnitude of delay mainly follows the profile of the transmission peaks. At the off-resonance wavelengths, the time delays are nearly zero. When a SPP resonance was excited, a relative longer delay has been observed. The pulse transmission time delay

through the single layer sample is about 60fs at the SPP resonance (Fig. 4a, *SL*). In the double layer samples, the relative time delays are about 100fs and 40-60fs at *SPP mode 1* and *SPP mode 2*, respectively (Fig. 4b-d, *D0*, *DY*, *DX*). The difference in the relative time delay curves for *DX* and *DY* configurations, especially around *SPP mode 2*, comes from the polarization dependence of the SPP excitations on the grating. FDTD simulations are also performed for both the transmission spectra and the pulse transmission time delay calculation (Fig. 5). Consistent with our experimental results, the FDTD simulation shows the simulated pulse delays vary with the pulse center wavelength and the magnitudes of the delays mainly follows the profiles of the optical transmission spectra. One obtains the largest pulse delay at the SPP resonance wavelengths. The relative pulse delays are calculated to be about 60-80fs at *SPP mode 1* and about 40-60fs at *SPP mode 2*, consistent with the experimental values.

C. SPP Lifetime

According to the Fano model,[26] The resonant peaks in the transmission spectra can be described in a form[11, 27, 28]

$$T_{Fano} = \left|t_B\right|^2 \frac{\left(1+\sum_r q_r/\varepsilon_r\right)^2}{1+\left(\sum_r \varepsilon_r^{-1}\right)^2}, \text{ with } \varepsilon_r = \frac{\omega-\left(\omega_{spp,r}+\Delta_r\right)}{\Gamma_r/2},\ q_r = \frac{2\delta_r}{\Gamma_r}, \qquad (1)$$

where $\left|t_B\right|^2$ is the non-resonant transmission coefficient, ω_{spp} is the angular frequency of the SPP excitation, Δ_r is the resonant shift originating from the coupling between the SPP state and the far-field continuum, Γ_r is the linewidth of the r^{th} SPP state which contains the radiative damping term due to the SPP-continuum coupling and the non-radiative damping terms such as the Ohmic losses in the metal. δ_r is the ratio between the resonant transition amplitude and the non-resonant transition.

The linewidth Γ of *SPP mode 1* is found to be about 41meV in a single layer structure (sample A, Fig. 4a) and about 25meV in the double layer structures (sample B and C, Fig. 4b-d), corresponding to a SPP lifetime (T_1) of 16fs and 26fs respectively. The linewidths of *SPP mode 2* are about 37meV and 29meV in Fig. 4c and Fig. 4d, corresponding to lifetimes of 18fs and 22fs, respectively. Compared to the SPP lifetime estimated from the transmission spectra, the measured pulse delay times are nearly 4 times larger. It should be noted that both *SPP mode 1* and *SPP mode 2* are the coupled modes of the whole structure instead of SPP excitations at single metal-dielectric interface. As in our experiments, single-interface SPPs excited at different aluminum surfaces combine to form coupled SPP 'super modes' in a similar way as in other coupled multiple-mode systems. Such super-modes are built up through the energy exchange between SPP excitations and the photons trapped in the structure, which requires sufficient interaction time.[29, 30] In systems with multiple interfaces, the time required to build up a super mode may be much longer than the life time of any modes involved, and thus leads to a longer pulse transmission time through the structure via the super-mode excitation.

D. SPP Coupling

To investigate the relation between the pulse delay and the lifetime of SPP mode, we study the transmission dynamics under the resonance condition using a simplified coupled-SPP-mode model. Of the two scattering channels, the contribution of the non-resonant channels is proportional to $(D/\lambda)^4$,[31] which is very small by subwavelength holes and will be ignored in our model. Figure 6 shows schematically the process of light transmission under the double-resonance condition:[30] the scattering of input state to the transmission continuum takes place with simultaneous

excitation of SPPs on two metal/dielectric interfaces. N_1 and N_2 are the field energy densities of the SPPs on the two coupled interfaces. $I(t)$ is the intensity of the incident pulse. *c* is speed of light in vacuum, and *n* is the reflective index of silicon oxide. Γ_{rad} and γ are the radiative and nonradiative damping of the SPP modes, associated with the line width of the SPP mode $\Gamma = \Gamma_{rad} + \gamma$. $\alpha\Gamma_{rad} N_i(t)$ is the portion of field energy density that coupled to the evanescent field in the hole channel per unit time, $(\alpha < 1)$, which induce energy transfer from N_i to N_j $(j \neq i)$ at time *t* while $S_{i\to j}(t)$ is the energy flux density per unit time arriving on N_j at time *t*.

Thus under the resonance condition the time-dependent equations describing the dynamics of the SPP-photon interaction are:

$$\begin{cases} \dfrac{dN_1(t)}{dt} = \dfrac{nI(t)}{c} - N_1(t)[(1-\alpha)\Gamma_{rad} + \gamma] - \alpha\Gamma_{rad} N_1(t) + S_{2\to 1}(t), \\ \dfrac{dN_2(t)}{dt} = -N_2(t)[(1-\alpha)\Gamma_{rad} + \gamma] - \alpha\Gamma_{rad} N_2(t) + S_{1\to 2}(t), \\ n\dfrac{T(t)}{c} = N_2(t)(1-\alpha)\Gamma_{rad}, \end{cases} \tag{2}$$

where $T(t)$ are the intensity of the transmitted pulse.

Because of the coupling between the SPPs on the two interfaces, temporal oscillations occur in the energy flow between N_1 and N_2 at a beating period of $T_{ex} = \pi/\Omega$, where $\Omega = \sqrt{\Delta\omega^2/4 + |V|^2} \approx |V|$, $|V|$ is the coupling strength, and $\Delta\omega$ is the detuning between the two SPPs on different interfaces.[21] Given the energy exchange yield [21] $\rho = |V/\Omega|^2$, the evanescence field density $\alpha\Gamma_{rad} N_1(t)$ flowing from N_1 arrived at N_2 after half of a period, among which a portion of ρ was transferred to N_2 whereas the rest $(1-\rho)$ was reflected back to N_1 after another half period, and so on. Thus the energy transferred from N_1 to N_2 at $t = t_0 \sim t_0 + \Delta t$ is

$$
\begin{aligned}
S_{1\to 2}(t_0)\Delta t &= \Delta t\cdot\alpha\Gamma_{rad}\left[N_1\left(t_0-\frac{1}{2}T_{ex}\right)\rho+N_1\left(t_0-\frac{3}{2}T_{ex}\right)\rho(1-\rho)^2+\cdots\right]\\
&\quad+\Delta t\cdot\alpha\Gamma_{rad}\left[N_2(t_0-T_{ex})\rho(1-\rho)+N_2(t_0-2T_{ex})\rho(1-\rho)^3+\cdots\right]\\
&=\Delta t\cdot\alpha\Gamma_{rad}\rho\left[\sum_{j=0}^{\infty}N_1\left(t_0-\left(j+\frac{1}{2}\right)T_{ex}\right)(1-\rho)^{2j}+\sum_{j=1}^{\infty}N_2(t_0-jT_{ex})(1-\rho)^{2j-1}\right]
\end{aligned}
\tag{3}
$$

where $N_i(t_0-t_a)$ is the field energy density of SPP mode on *interface i* at $(t=t_0-t_a)$. If the asymmetry in the hole arrays between the bottom and top surfaces of each aluminum layer was ignored, one obtains $\Delta\omega\approx 0$. It follows $\rho=|V/\Omega|^2\approx 1$. Thus only the first term in the summary in Eq. (3) is nonzero, i.e.

$$
S_{1\to 2}(t_0)\Delta t\approx\Delta t\cdot\alpha\Gamma_{rad}N_1\left(t_0-\frac{1}{2}T_{ex}\right). \tag{4}
$$

Since the emitted photons from SPPs are radiated in both the forward and the backward direction, we assume one half of the radiation is coupled to the far field scattering states whereas the other half towards the hole channels contributing to the energy exchange between N_1 and N_2, i.e. $\alpha=1/2$. Equations (2) are then reformed to

$$
\begin{cases}
\dfrac{dN_1(t)}{dt}=\dfrac{nI(t)}{c}-N_1(t)(\Gamma_{rad}+\gamma)+N_2\left(t-\dfrac{1}{2}T_{ex}\right)\Gamma_{rad}/2,\\
\dfrac{dN_2(t)}{dt}=-N_2(t)(\Gamma_{rad}+\gamma)+N_1\left(t-\dfrac{1}{2}T_{ex}\right)\Gamma_{rad}/2,\\
\dfrac{n}{c}T(t)=N_2(t)\Gamma_{rad}/2.
\end{cases}
\tag{5}
$$

Hence the transmitted pulse $T(t)$ can be calculated and the pulse delays T_{delay} are then estimated from the peak-to-peak time lag between the incident pulse $I(t)$ and the transmitted pulse $T(t)$ (Fig. 7). Figure 8 shows the contour line plot of the calculated pulse delay T_{delay} as a function of both the SPP lifetime T_1 and the field energy exchange period T_{ex}. In the calculation, both T_1 and T_{ex} have been considered

as free parameters. The longer pulse delays correspond to larger T_1 and T_{ex}. The experimental data for different configurations (squared symbols) are also plotted on the contour map, whose SPP lifetime T_1 was retrieved from the Fano line-shape fitting of the corresponding transmission peak and the pulse delays T_{delay} is from the measurement. Thus the y-coordinates of the squared symbols indicate the value of T_{ex} and consequently indicate the coupling strength between the SPPs on different interfaces in each structure.

With the coupled-SPP-mode transmission model, T_{ex} is estimated to be about 40fs in the single-layered sample and about 80-100fs in the double-layered sample for *SPP mode 1*, corresponding to a coupling strength of 52meV and 23meV, respectively (Fig. 8). As we mentioned before, the surface charge oscillation at *SPP mode 1* is confined on the two outer Al/SiO_2 interfaces, suggesting the transmission at *SPP mode 1* is mediated via the coupling of the SPPs on these two outer Al/SiO_2 interfaces. The doubled T_{ex} in the double-layered structures reflects the relative weak coupling due to the doubled film thickness. For *SPP mode 2*, the estimated T_{ex} (15fs in DY configuration and 40fs in DX configuration) is much smaller than that of *SPP mode 1* in the double-layered samples. It suggests a stronger interaction between SPP waves at the two inner interfaces upon the excitation of *SPP mode 2*, associated with the localized electromagnetic field in the dielectric gap between the aluminum layers. Compared to the DY configuration, the localized field intensity is lower in the DX case due to the x-directional shift between the upper and lower hole arrays [23]. Accordingly, the electromagnetic coupling between the two inner interfaces is relatively smaller in the DX configuration, which is consistent with our coupled-mode model calculation (Fig.8). Since the incident pulse duration in the measurement was

twice of the estimated energy exchange period T_{ex} at the two SPP resonances, the oscillation feature due to periodic energy exchange was not resolved in the temporal evolution of the transmitted pulse in our experiments (Fig. 2).

E. Nonradiative SPP Damping

Eqs. (2-5) discussed above is only applicable to the case of weak coupling where SPPs on single interface are nearly unchanged. This is justified for *SPP mode 1* in our samples. However for *SPP mode 2*, the resonant coupling occurs between the two inner Al/SiO2 interfaces and the field extension is about 3μm in SiO2, which is much larger than the dielectric gap (300nm) between the two interfaces. Thus the small-perturbation approximation may not be appropriate. Here we consider $N_S = (N_1 + N_2)/2$ as a combined SPP mode of N_1 and N_2 in the whole structure. Thus Eqs. (2) are reformed as

$$\begin{cases} \dfrac{dN_S(t)}{dt} = \dfrac{nI(t)}{2c} - N_S(t)(\Gamma_{rad}/2 + \gamma), \\ \dfrac{n}{c}T(t) = N_S(t)\Gamma_{rad}/2, \end{cases} \tag{6}$$

which suggests the combined system reacts like a super SPP mode but with a radiative damping term, $\Gamma_{rad}/2$, half of that on an isolated interface. This also suggests the nonradiative term γ, for example the Ohmic loss, will have stronger effect in the transmission process at the *SPP mode 2*. This result is consistent with the FDTD simulation. As shown in Fig. 9, by reducing $\mathrm{Im}(\varepsilon_{Al})$ to 1/10 of the original value (ε_{Al} is the dielectric function of aluminum and $\mathrm{Im}(\chi)$ is the imaginary part of χ), the linewidth of *SPP mode 2* decreases from 38meV to 16meV while the linewidth of *SPP mode 1* decreases from 25meV to 23meV. Moreover, the resonance peak at *SPP mode 2* is largely suppressed as the losses increase to ten times of the original value.

This also explains the relative lower transmission amplitude at the *SPP mode 2* in our experiments.

IV. SUMMARY

In summary, we have measured the pulse delays through single- and double-layered aluminum films perforated with hole arrays using an up-conversion technique. The frequency-dependent pulse transmission time delay mainly follows the profile of the transmission spectra. The maximum temporal delays at the SPP resonances are about 60fs and 100fs for the single layer and the double layer samples respectively, which is consistent with the FDTD simulations. A coupled-SPP-mode transmission model is used to understand the temporal dynamics of pulse propagation through hole arrays via the interactions between SPPs on different interfaces. According to the measured time delays, we deduce that the coupling strength between the two outer Al/SiO_2 interfaces is about 52meV and 23meV in the single- and double-layered samples. The coupling strength between the two inner Al/SiO_2 interfaces is much stronger which leads to a fast energy exchange between the SPPs on these two interfaces and a relative shorter pulse delay upon the excitation of *SPP mode 2*. The longer temporal delays of light pulses achieved by weakly coupled metal/dielectric interfaces may help improving the performance of nanoscale plasmonic structures and designing new photonic devices.

Acknowledgement: This work was supported by the Research Grants Council of Hong Kong (Project No. 603908 and 600308) and part of the computational work was conducted using the resources of the High Performance Cluster Computing Centre in

the Hong Kong Baptist University. ZM and HBC are supported by the National Science Foundation ECS-0621944.

[1] T. W. Ebbesen, H. J. Lezec, H. F. Ghaemi, T. Thio, and P. A. Wolff, Nature **391**, 667 (1998).

[2] C. Ropers, T. Elsaesser, G. Cerullo, M. Zavelani-Rossi, and C. Lienau, New J. Phys. **9**, 397 (2007).

[3] A. Agrawal, H. Cao, and A. Nahata, New J. Phys. **7**, 249 (2005).

[4] E. Hendry, M. J. Lockyear, J. G. Rivas, L. Kuipers, and M. Bonn, Phys. Rev. B **75**, 235305 (2007).

[5] S. A. Maier, IEEE J. Sel. Top. Quantum Electron. **12**, 1214 (2006).

[6] X. G. Luo and T. Ishihara, Appl. Phys. Lett. **84**, 4780 (2004).

[7] M. E. Stewart, C. R. Anderton, L. B. Thompson, J. Maria, S. K. Gray, J. A. Rogers, and R. G. Nuzzo, Chem. Rev. **108**, 494 (2008).

[8] M. C. Tam, H. M. Su, K. S. Wong, X. L. Zhu, and H. S. Kwok, Appl. Phys. Lett. **95**, 051503 (2009).

[9] W. L. Barnes, A. Dereux, and T. W. Ebbesen, Nature **424**, 824 (2003).

[10] A. V. Zayats and Smolyaninov, II, J. Opt. A-Pure Appl. Opt. **5**, S16 (2003).

[11] C. Genet, M. P. van Exter, and J. P. Woerdman, Opt. Commun. **225**, 331 (2003).

[12] A. Dogariu, T. Thio, L. J. Wang, T. W. Ebbesen, and H. J. Lezec, Opt. Lett. **26**, 450 (2001).

[13] T. H. Isaac, W. L. Barnes, and E. Hendry, Phys. Rev. B **80**, 115423 (2009).

[14] C. Ropers, D. J. Park, G. Stibenz, G. Steinmeyer, J. Kim, D. S. Kim, and C. Lienau, Phys. Rev. Lett. **94**, 113901 (2005).

[15] C. Ropers, et al., Appl. Phys. B-Lasers Opt. **84**, 183 (2006).

[16] A. S. Vengurlekar, A. V. Gopal, and T. Ishihara, Appl. Phys. Lett. **89**, 181927 (2006).

[17] R. V. Andaloro, H. J. Simon, and R. T. Deck, Appl. Optics **33**, 6340 (1994).

[18] P. N. Stavrinou and L. Solymar, Phys. Rev. E **68**, 066604 (2003).

[19] R. Muller, V. Malyarchuk, and C. Lienau, Phys. Rev. B **68**, 205415 (2003).

[20] A. Dechant and A. Y. Elezzabi, Appl. Phys. Lett. **84**, 4678 (2004).

[21] R. Muller, C. Ropers, and C. Lienau, Opt. Express **12**, 5067 (2004).

[22] R. Rokitski, K. A. Tetz, and Y. Fainman, Phys. Rev. Lett. **95**, 177401 (2005).
[23] Z. Marcet, et al., Opt. Lett. **35**, 2124 (2010).
[24] Y. Li, H. Su, K. S. Wong, and X.-Y. Li, J. Phys. Chem. C **114**, 10463 (2010).
[25] K. S. Wong, H. Wang, and G. Lanzani, Chemical Physics Letters **288**, 59 (1998).
[26] U. Fano, Physical Review **124**, 1866 (1961).
[27] S. H. Chang, S. K. Gray, and G. C. Schatz, Opt. Express **13**, 3150 (2005).
[28] M. Sarrazin, J.-P. Vigneron, and J.-M. Vigoureux, Phys. Rev. B **67**, 085415 (2003).
[29] L. Martin-Moreno, F. J. Garcia-Vidal, H. J. Lezec, K. M. Pellerin, T. Thio, J. B. Pendry, and T. W. Ebbesen, Phys. Rev. Lett. **86**, 1114 (2001).
[30] S. A. Darmanyan and A. V. Zayats, Phys. Rev. B **67**, 035424 (2003).
[31] H. A. Bethe, Physical Review **66**, 163 (1944).

FIG. 1 (color online) (a) Demonstration diagram of the double layer aluminum film perforated with subwavelength hole arrays. The lateral shift L_x is 0 in sample B and 0.5μm in sample C. (b) Scheme of the up-conversion setup for pulses transmission time delay measurement.

FIG. 2 (color online) The up-converted signal with incident light pulse at 1.548μm in the cases of: pulse propagated in air (open squares, refers to the **x**-axis on the top), through bare substrate without aluminum layers (solid curve in black), through sample A (line with squares in purple, *SL*), through sample B (open circles in red, *D0*), through sample C with incident field polarized perpendicular to the lateral shift between the upper and lower aluminum layers (solid circles in blue, *DY*), through

sample C with incident field polarized parallel to the lateral shift (triangles in green, *DX*). The inset shows the spectrum of the incident pulse.

FIG. 3 (color online) FDTD simulation on the near-filed H_x components of *SPP mode 1* in sample B (a) and sample C (c); *SPP mode 2* in sample B (b) and sample C (d). The structures were illuminated from the bottom side. Please note that the color-maps for the two modes are different for the reason of clarity.

FIG. 4 (color online) Measured time delays of light pulse centered at different wavelength through sample A (a), sample B (b), and sample C with incident light polarized perpendicular (c) or parallel (d) to the lateral shift between the hole arrays in the two layers. Black solid lines are the measured far-field transmission spectra of each sample. The dash curves are the Fano profile fittings on the transmission spectra according to Eq. (1). The square scatters are the delay time extracted from the up-conversion measurement by taking the pulse propagation delay through the substrate as reference.

FIG. 5 (color online) Simulated transmission spectra (solid line) and simulated delay time (line with squares) for each case as in Fig.4.

FIG. 6 (color online) Schematic of transmission through hole arrays via coupled SPP modes.

FIG. 7 (color online) Simulations on the transmitted pulse profile through sample A (*SL*) and sample B (*D0*) at the *SPP mode 1*. The incident pulse width is 150fs.

Parameters of $(T_1 = 16\,fs, T_{ex} = 40\,fs)$ and $(T_1 = 26\,fs, T_{ex} = 85\,fs)$ have been used in the *SL* configuration and the *D0* configuration, respectively. The transmitted pulse profiles are multiplied by a factor of 2 for the reason of clarity.

FIG. 8 (color online) Contour line plot of the pulse transmission time delay T_{delay} as a function of SPP lifetime T_1 and energy exchange period T_{ex} between the coupled SPPs, calculated from Eq. (3). The curves labeled from 35fs to 95fs are the calculated pulse delays. Square symbols: the measured pulse delays at *SPP mode 1* and *mode 2* for *sample A* (*SL*, SPP1), *sample B* (*D0*, SPP1), *sample C* with incident light polarized along the lateral shift (*DX*, SPP1, SPP2) and perpendicular to the lateral shift (*DY*, SPP1, SPP2). The positions of the symbols are according to the measured pulse delays T_{delay} and the SPP lifetime T_1 estimated from the FWHM of the resonance peaks in the transmission spectra.

FIG. 9 (color online) FDTD simulation on the transmission spectra for aligned double-layer hole array structure with different loss. For simplicity, the imaginary parts of the dielectric function of aluminum were multiplied by a factor of 0.1, 1.0, and 10 in each case. The "10 Loss" curve is multiplied by 2 for the sake of clarity. The linewidths of each resonance peak are estimated by fitting to the Fano model [Eq. (1)].

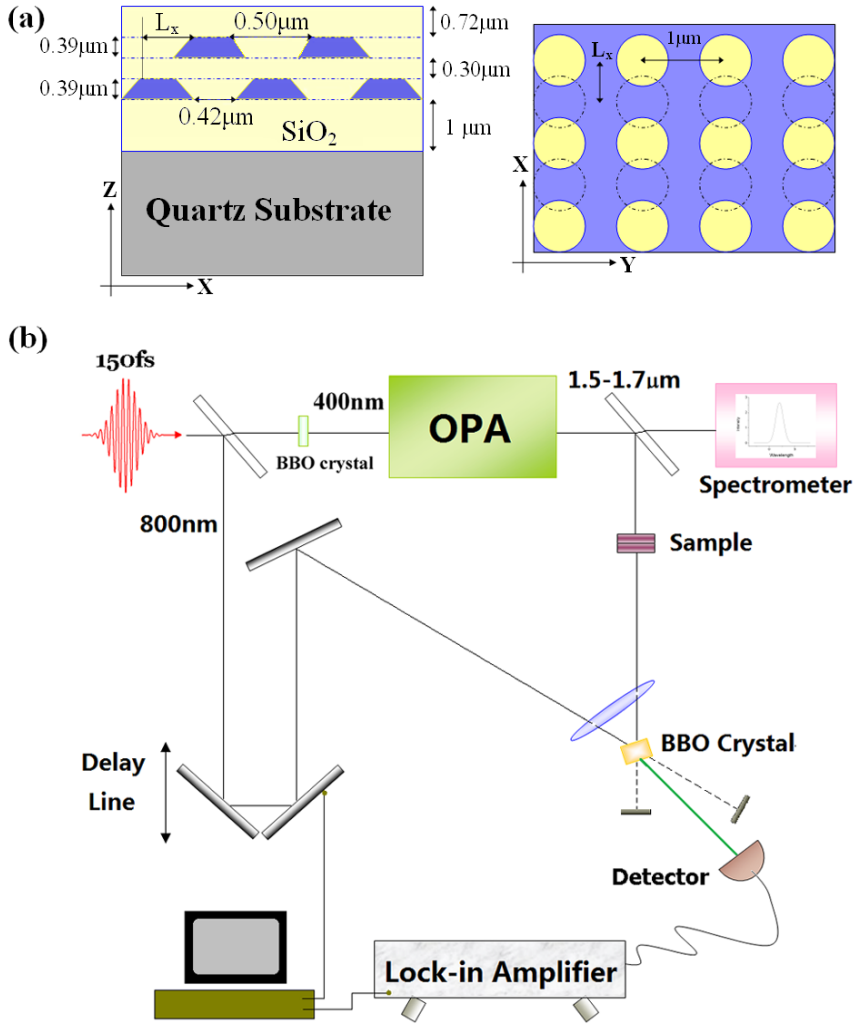

FIG. 1 H.M. Su, Z.H. Hang, Z. Marcet, H.B. Chan, C.T. Chan, K.S. Wong

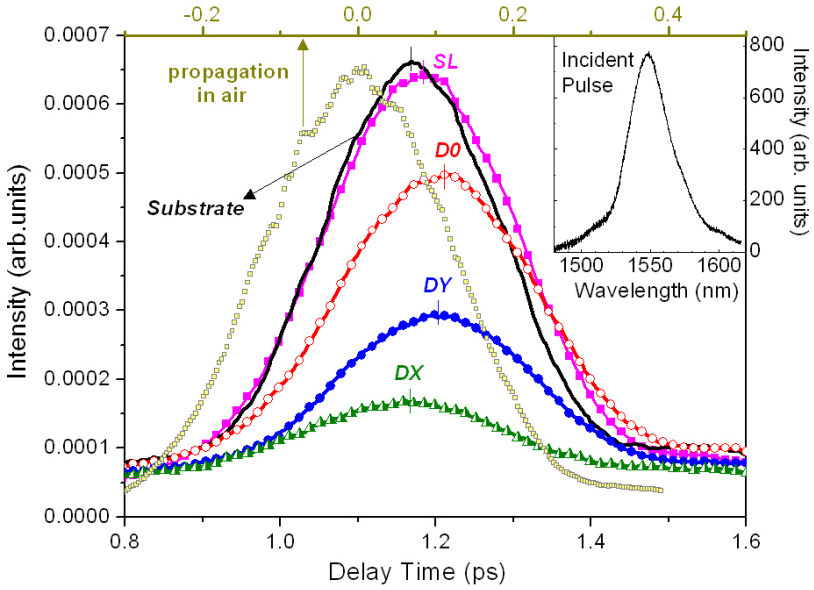

FIG. 2 H.M. Su, Z.H. Hang, Z. Marcet, H.B. Chan, C.T. Chan, K.S. Wong

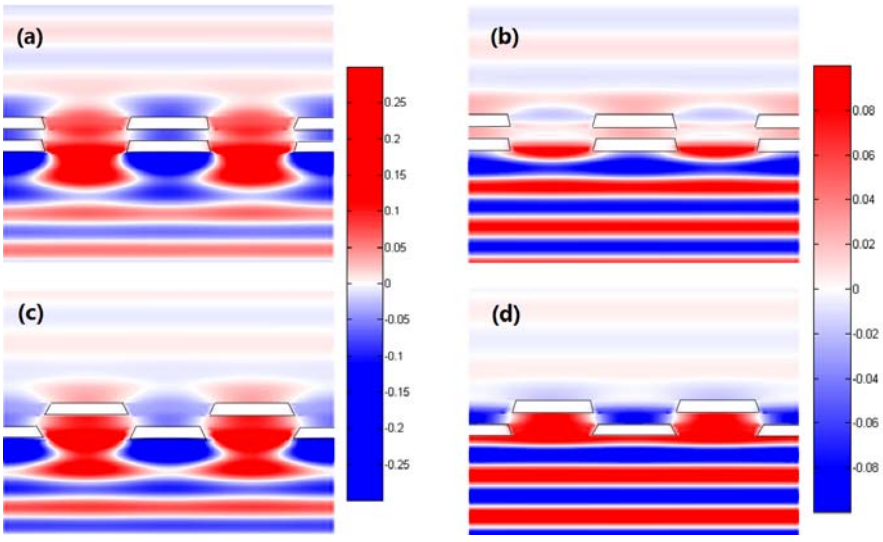

FIG. 3 H.M. Su, Z.H. Hang, Z. Marcet, H.B. Chan, C.T. Chan, K.S. Wong

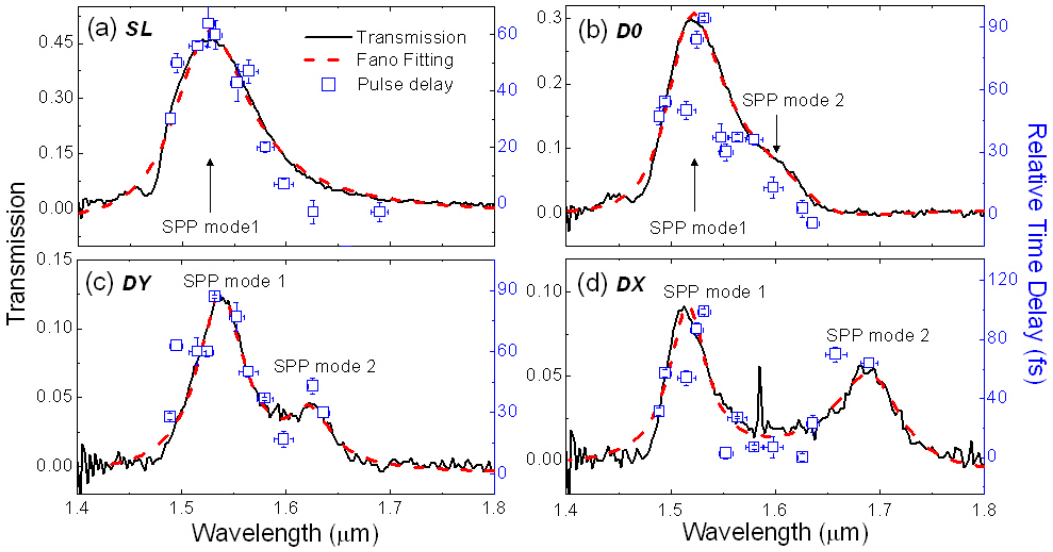

FIG. 4 H.M. Su, Z.H. Hang, Z. Marcet, H.B. Chan, C.T. Chan, K.S. Wong

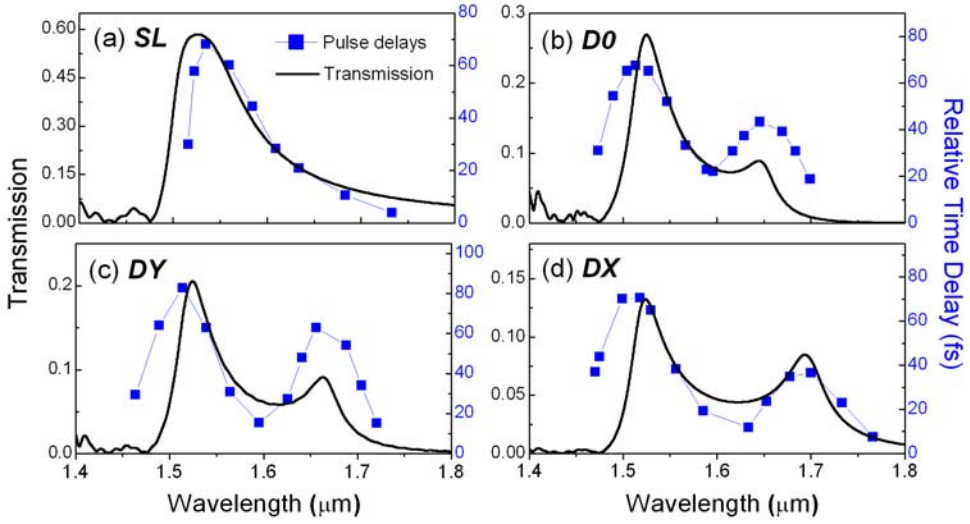

FIG. 5 H.M. Su, Z.H. Hang, Z. Marcet, H.B. Chan, C.T. Chan, K.S. Wong

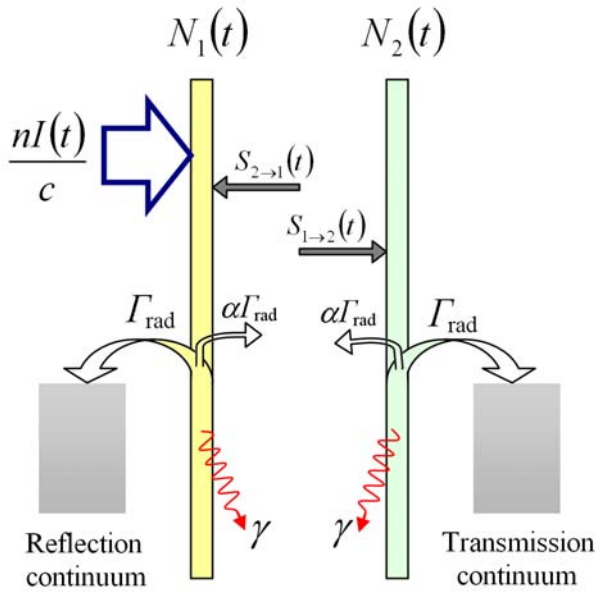

FIG. 6 H.M. Su, Z.H. Hang, Z. Marcet, H.B. Chan, C.T. Chan, K.S. Wong

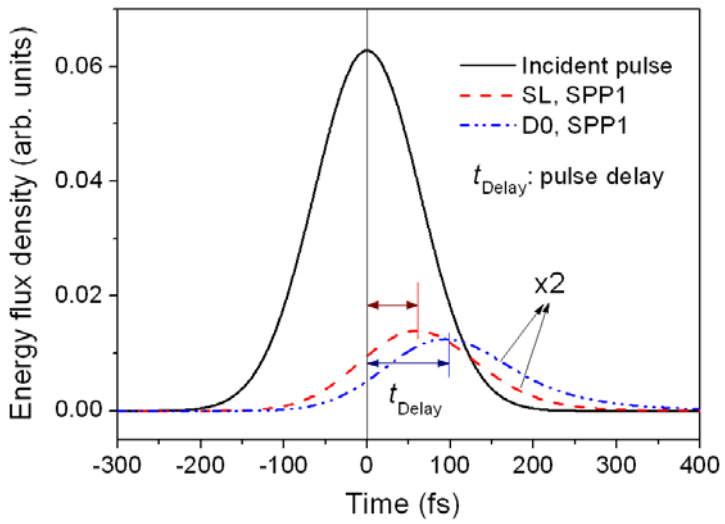

FIG. 7 H.M. Su, Z.H. Hang, Z. Marcet, H.B. Chan, C.T. Chan, K.S. Wong

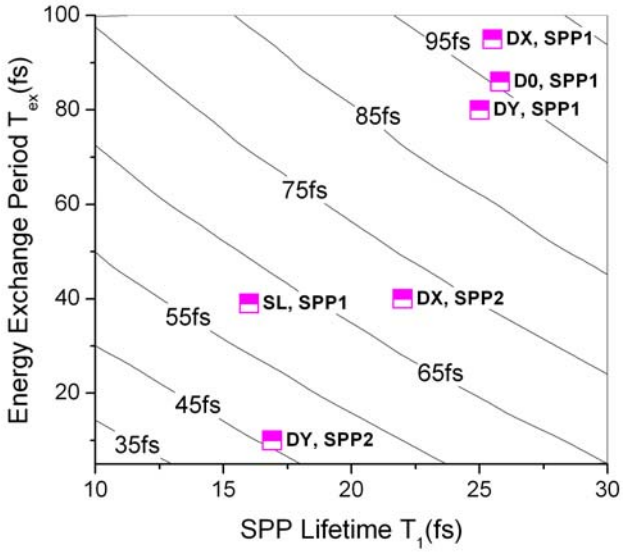

FIG. 8 H.M. Su, Z.H. Hang, Z. Marcet, H.B. Chan, C.T. Chan, K.S. Wong

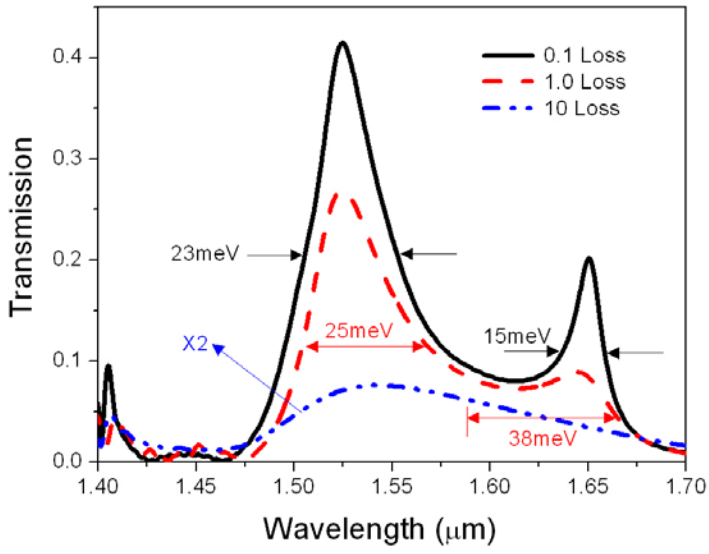

FIG. 9 H.M. Su, Z.H. Hang, Z. Marcet, H.B. Chan, C.T. Chan, K.S. Wong